THE JOURNAL OF PHYSICAL CHEMISTRY A

pubs.acs.org/JPCA Article

Balancing Charge Transfer and Frenkel Exciton Coupling Leads to Excimer Formation in Molecular Dimers: Implications for Singlet Fission

Published as part of The Journal of Physical Chemistry virtual special issue "Josef Michl Festschrift".

Youn Jue Bae, Daiki Shimizu, Jonathan D. Schultz, Gyeongwon Kang, Jiawang Zhou, George C. Schatz, Atsuhiro Osuka, and Michael R. Wasielewski*

Cite This: *J. Phys. Chem. A* 2020, 124, 8478–8487 Read Online

ACCESS | Metrics & More | Article Recommendations | Supporting Information

ABSTRACT: Photoexcitation of molecular chromophore aggregates can form excimer states that play a significant role in photophysical processes such as charge and energy transfer as well as singlet fission. An excimer state is commonly defined as a superposition of Frenkel exciton and charge transfer states. In this work, we investigate the dynamics of excimer formation and decay in π-stacked 9,10-bis(phenylethynyl)anthracene (BPEA) covalent dimers appended to a xanthene spacer, where the electronic coupling between the two BPEA molecules is adjusted by changing their longitudinal molecular slip distances. Using exciton coupling calculations, we quantify the relative contributions of Frenkel excitons and charge transfer states and find that there is an upper and lower threshold of the charge transfer contribution for efficient excimer formation to occur. Knowing these thresholds can aid the design of molecular aggregates that optimize singlet fission.

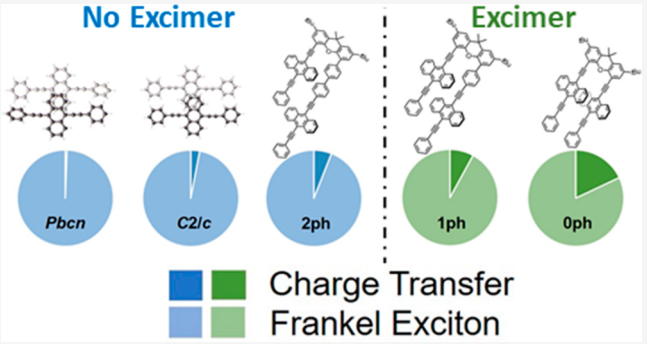

INTRODUCTION

Photoexcitation of molecular chromophore aggregates often results in the formation of excimer states in which an exciton on one chromophore electronically interacts with one or more neighboring chromophores, resulting in overall stabilization of the system.[1] Excimer formation is observed in various types of chromophore assemblies including covalent dimers,[2−5] aggregates in solution,[6−8] and in the solid state,[9] which is of particular interest to organic electronics[10,11] and photovoltaics.[12,13] Often times, excimer states can act as an exciton traps[14] and decrease the quantum yield of desired products or device performance.[15] This occurs when the excimer formation rate is faster than the targeted processes such as exciton diffusion, charge transfer and transport, and singlet fission (SF).[16,17] However, in some cases, excimers have been proposed to act as intermediates in desirable photophysical process, for example, to mediate SF in polycrystalline 3,6-bis(aryl)diketopyrrolopyrrole (DPP) films[18] and perylene-3,4:9,10-bis(dicarboximide) (PDI) covalent dimers.[19] Traditionally, the excimer state has been defined as a linear combination of Frenkel exciton (FE) and charge transfer (CT) states. Defining $|S_1S_0\rangle$ and $|S_0S_1\rangle$ as states where the excitation resides on one of the two molecules and $|AC\rangle$ and $|CA\rangle$ where the cation and anion reside on either molecule, the excimer state, $|Ex\rangle$, can be expressed as[20]

$$|Ex\rangle = a(|S_1S_0\rangle+|S_0S_1\rangle) + b(|CA\rangle+|AC\rangle)$$

where a and b are coefficients and the squares of these coefficients indicate the relative contributions of the FE and CT states. The relative degree to which the FE and CT states contribute to $|Ex\rangle$ depends on the electronic interactions in molecular aggregates as dictated by the interchromophore distance, orientation, and solvation environment.[21,22]

The contribution from the FE state can be understood as the Coulombic interactions among the molecules comprising the aggregates as described by the Kasha model.[23] These Coulombic interactions are dictated by the relative orientations of transition dipole moments and result in Davydov splitting, which can be easily observed in the steady state absorption spectra of the aggregates.[24] Contributions of the CT state to the excimer state have been widely recognized from the observed solvent polarity dependence of excimer formation.[5,6,21,22] In many systems, having large CT character

Received: August 21, 2020
Revised: September 23, 2020
Published: September 25, 2020

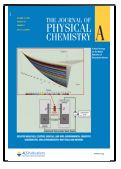

https://dx.doi.org/10.1021/acs.jpca.0c07646
J. Phys. Chem. A 2020, 124, 8478–8487

stabilizes the excimer state, resulting in faster excimer formation in higher yield. For instance, in the case of extended viologens, a shorter distance between the two chromophores leads to increased CT character and thus faster excimer formation,[22] while for PDI dimers and aggregates, excimers with increased CT character have been observed in highly polar solvents.[6,21] Recently, folded geometries of PDI dimers were shown to have similar CT and FE contributions based on their calculated exciton couplings.[5,25] It has also been reported that a CT contribution comparable to that of the FE state allows for SF leading to $^1(T_1T_1)$ multiexciton state formation.[21] Although it is widely assumed that most excimer states have a large FE contribution with a small degree of CT character that stabilizes the excimer state, it remains unclear what degree of CT state contribution relative to the FE states is necessary to facilitate or avoid excimer formation, leading to important implications for the role of excimers in other photophysical processes, such as SF.

Here, we synthesized covalent dimers of 9,10-bis(phenylethynyl)anthracene (BPEA) using a xanthene bridge and a phenylene spacer (Scheme 1) to systematically tune the electronic coupling between two BPEA molecules and to study their excited state dynamics. BPEA is an extensively studied industrial dye that has a near unity fluorescence quantum yield in solution. Recently, it has been shown that BPEA in the solid state undergoes efficient SF.[26−28] However, we found that excimer formation is the dominant photophysical process in covalent BPEA dimers based on solvent-dependent transient absorption and time-resolved fluorescence studies. In addition to the experimental studies, we calculated the exciton couplings to quantify the contribution of FE and CT states in BPEA and other systems including PDI covalent dimers and polycrystalline DPP systems. Such calculations show a correlation between excimer formation dynamics and the relative ratio of FE to CT state contribution to the overall electronic description of the excimer.

Scheme 1. BPEA Covalent Dimers 0ph, 1ph, and 2ph

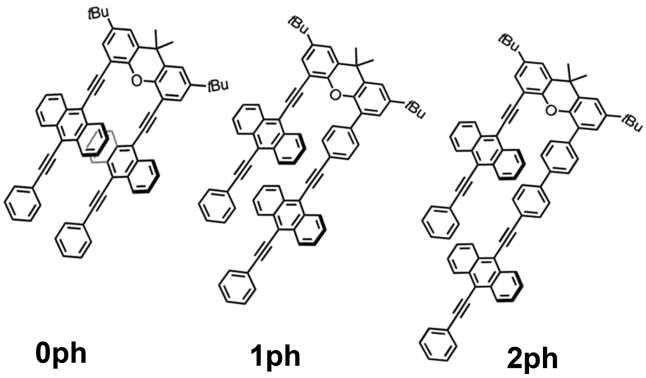

EXPERIMENTAL SECTION

Synthesis of BPEA Dimers. The BPEA covalent dimer **0ph** was synthesized by Sonogashira coupling of 4,5-dibromo-2,7-di-*tert*-butyl-9,9-dimethylxanthene and 9-ethynyl-10-phenylethynylanthracene in 27% yield. The reaction also gave monosubstituted xanthene **S1** in 67% yield, which was used to prepare slip-stacked **1ph** and **2ph**. Namely, **1ph** and **2ph** were synthesized by Suzuki−Miyaura coupling of **S1** and the corresponding boronic esters **S4** and **S5**, respectively (Scheme 2, see the Supporting Information for detailed procedures).

Spectroscopy. UV−vis absorption spectra were acquired in toluene (Tol), dichloromethane (DCM), and *N*,*N*-dimethylformamide (DMF) on a Shimadzu UV1800 absorption spectrometer. Emission spectra were collected by using a Horiba Nanolog spectrofluorometer. Fluorescence quantum yields, Φ_F, were determined by using the front-face mode with a HORIBA Nanolog spectrofluorometer equipped with an integrating sphere (Horiba Quanta-φ).

The femtosecond transient absorption (fsTA) experiments were conducted by using instruments described previously.[29] The 414 nm pump pulses were generated by using a laboratory-built collinear optical parametric amplifier and attenuated to 1 μJ/pulse.[30] The pump pulses were depolarized to suppress the effects of orientational dynamics. Transient absorption spectra were detected by using a customized Helios/EOS spectrometer (Ultrafast Systems, LLC), where the Helios spectrometer is used for pump−probe delays up to 7.4 ns and the EOS spectrometer is used for pump−probe delays

Scheme 2. Synthesis of Covalent BPEA Dimers 0ph, 1ph, and 2ph

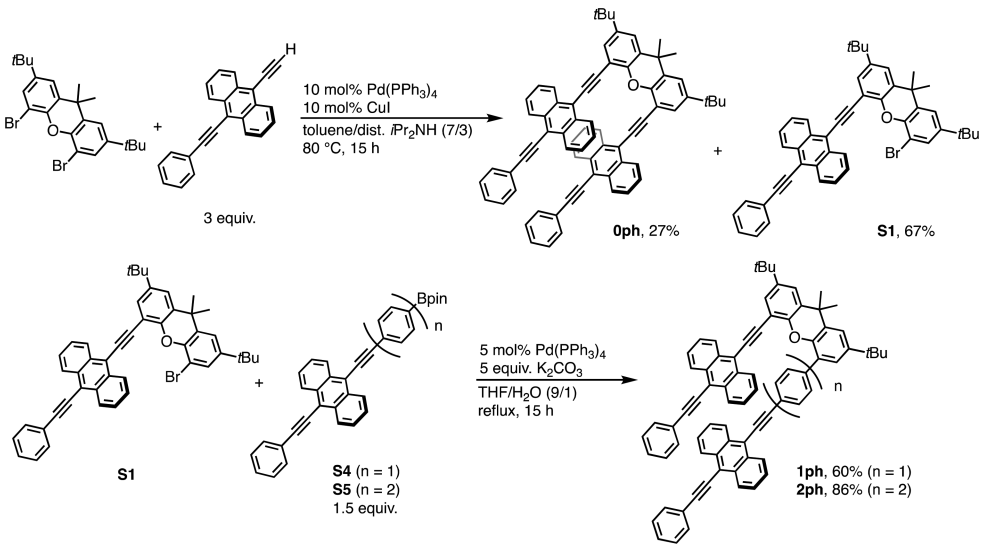

https://dx.doi.org/10.1021/acs.jpca.0c07646
J. Phys. Chem. A 2020, 124, 8478−8487

of 0.6 ns−340 μs. The optical density of the samples was ∼0.3 at the excitation wavelength (λ_{ex} = 414 nm) in 2 mm cuvettes.

Picosecond time-resolved fluorescence (psTRF) data were collected by using a Hamamatsu C4780 streak camera. The 414 nm, 15 nJ laser pulses from a Spirit-NOPA-3H were utilized as the excitation source. Data were collected by using 2, 10, and 100 ns time windows; the instrument response function (IRF) was ∼2% of the acquisition window, with the highest time resolution being 40 ps. The IRF was determined from the pump scatter by using Gaussian deconvolution as described in the Supporting Information. The optical density of the samples was kept below 0.1 at the excitation wavelength in 2 mm cuvettes. All data were acquired in the single-photon counting mode by using the Hamamatsu HPD-TA software.

Exciton Coupling (*J*) Calculations. The value of J is calculated by simulating the steady state absorption spectra of the BPEA compounds through time propagation of the Frenkel/charge transfer Holstein Hamiltonian.[31,32] This Hamiltonian captures how the presence and mixing of exciton and CT states impact the linear response of the compound. We use a single Franck−Condon-active vibration to describe the nuclear degrees of freedom for both the singlet and CT manifolds. To capture the spectral line widths, we apply a Gaussian windowing function to the time-domain linear response prior to Fourier transformation to the frequency domain. We first simulated the BPEA monomer spectrum to extract a Huang−Rhys factor of ∼0.9 for the primary ∼1400 cm^{-1} vibration apparent in the vibronic structure of the experimental spectra. This C═C stretch has been previously studied in anthracene-based compounds.[33,34] We used this result in conjunction with the calculated electron and hole transfer integrals to simulate the dimer linear responses and determine the strength of the Coulombic interaction between the BPEA chromophores. Further details regarding these simulations can be found in the Supporting Information.

The hole and electron transfer integrals between HOMO−HOMO and LUMO−LUMO of the two molecules were calculated from the integral matrix elements by using the Amsterdam Density Functional (ADF) package[35] at the density functional level of theory (DFT). Here, the BPEA dimers are geometry optimized in dichloromethane (DCM) by using B3LYP basis and Grimme3 dispersion correction functional to account for $\pi-\pi$ interactions. Optimized structures are shown in Figure S24. Following the optimization, the xanthene bridge was removed similar to the method used for previous systems[36] to calculate the transfer integrals. For calculating the one-electron coupling, the triple ζ with two polarization functions (TZ2P) basis set and the B3LYP exchange-correlation functional were chosen. Fock and overlap integral matrix elements were calculated by using the TRANSFERINTEGRALS key with the fragment orbital approach as implemented in ADF. The effective coupling between orbitals i and f, V_{if}, was calculated via the following equation:[37]

$$V_{if} = \frac{J_{if} - \frac{1}{2}S_{if}(e_i + e_f)}{1 - {S_{if}}^2} \quad (1)$$

where J_{if} is the Fock matrix element between a pair of monomers, S_{if} is the overlap integral, and e_i and e_f are the Fock matrix elements within a monomer. The calculated matrix elements for the corresponding systems are shown in Table S2.

The CT state energy, E(CT), was calculated by performing a single-point energy calculation using density functional theory (DFT) calculations. Geometries of BPEA and PDI monomers (Figure 5) were optimized in QChem (v. 5.0) with the B3LYP functional and 6-31G* basis set in the gas phase followed by further optimization using a polarizable continuum model (C-PCM) and the specified optical and static dielectric constants for each solvent medium. A single-point energy calculation on the optimized geometry was performed, and convergence was reached to obtain the energy of neutral, anion, and cation species. The energy of the anion and cation is scaled by subtracting the energy of neutral species, and the E(CT) was calculated as the sum of cation and anion energy.[38,39] Example input files and the values are reported in Table S3.

RESULTS

Steady State Optical Properties. Ground state absorption spectra of the covalent BPEA dimers in DCM were obtained to qualitatively compare exciton coupling among BPEA dimers (Figure 1). The absorption maxima of 0−0 and

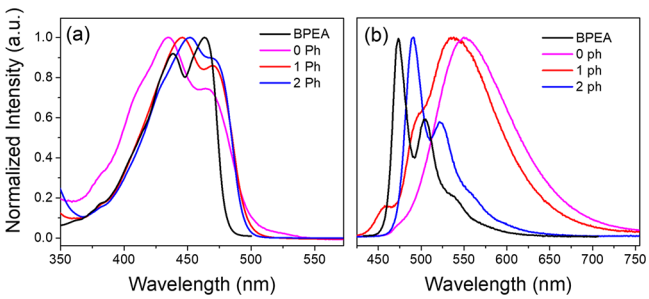

Figure 1. (a) Steady state absorbance and (b) emission spectra of BPEA monomer and dimers in DCM.

0−1 transitions in BPEA monomer in DCM are 464 and 438 nm, respectively, and the 0−0 transition has a greater intensity than the 0−1 transition. Because of multiple conformers in the solution phase, the BPEA monomer in solution has a broad absorption.[40] Unlike the BPEA monomer, the 0−1 transitions in the BPEA covalent dimers have greater intensities than the 0−0 transitions, indicating H-type intramolecular interactions.[24] Presumably, strong $\pi-\pi$ interactions drive the BPEA molecules to stack even with phenyl spacers. The absorption maxima of the 0−0 and 0−1 bands of **0ph** are 466 and 435 nm, respectively, which are comparable to the BPEA monomer. In contrast, the 0−0 and 0−1 transitions of both **1ph** and **2ph** are red-shifted (Table 1). Steady state absorbance spectra of the BPEA dimers in Tol are shown in Figure S1 with the corresponding peak positions and Φ_F (Table S1).

The steady state fluorescence spectrum of the BPEA monomer in DCM has a clear vibronic progression of 0−0,

Table 1. Absorption and Emission Maxima, Singlet State Energies ($E(S_1)$), and Fluorescence Quantum Yields of BPEA Monomer and Dimers in DCM

	0−0 (nm)	0−1 (nm)	$E(S_1)$ (eV)	Φ_F (%)
BPEA	464	438	2.60	95 ± 5
0ph	466	435	2.52	59 ± 3
1ph	471	446	2.55	92 ± 7
2ph	473	452	2.57	82 ± 9

https://dx.doi.org/10.1021/acs.jpca.0c07646
J. Phys. Chem. A 2020, 124, 8478−8487

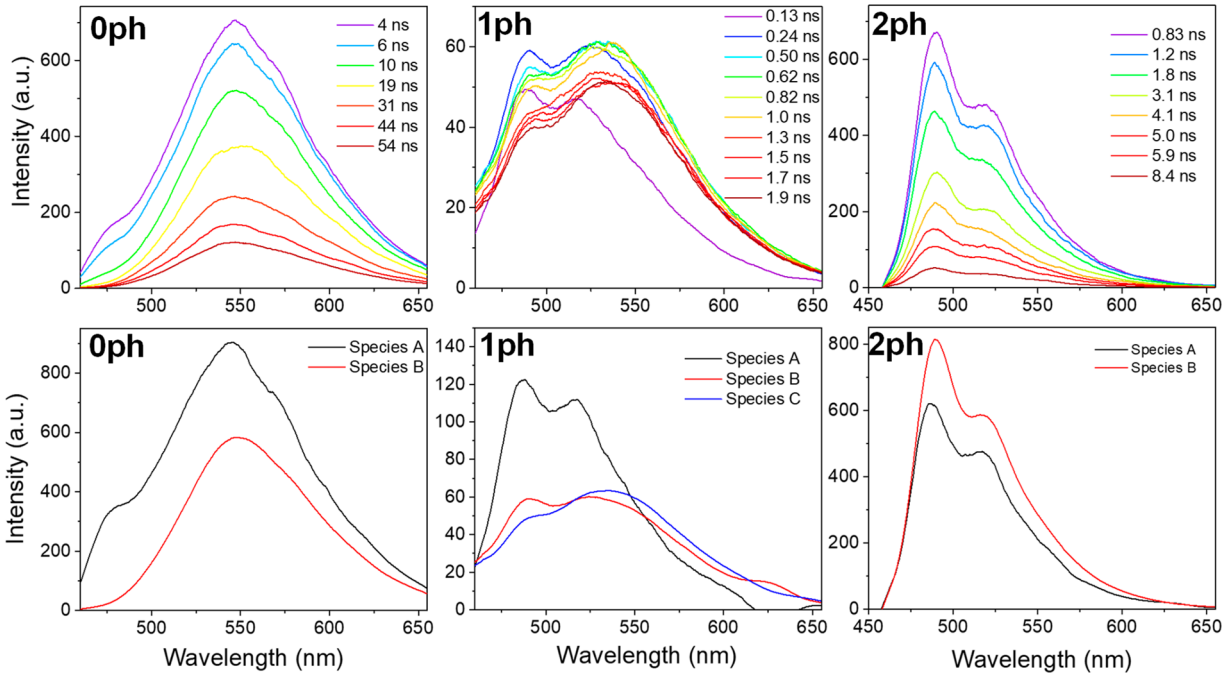

Figure 2. TRF spectra of BPEA dimers in DCM upon photoexcitation at λ_{ex} = 414 nm (15 nJ/pulse). The TRF spectra are globally fit by using an A → B → C → GS evolution-associated decay model, and the resulting spectral fits are shown in the bottom panel. Additional time windows, wavelength fits, and population vs time fits are shown in Figures S3−S12.

Table 2. Excimer Formation and Decay Time Constants from TRF Measurements for BPEA Dimers in DCM and Tol

	0ph DCM	**0ph** Tol	**1ph** DCM	**1ph** Tol	**2ph** DCM	**2ph** Tol
τ_1	50 ± 40 ps	1.7 ± 0.2 ns	27 ± 40 ps	220 ± 40 ps	200 ± 40 ps	510 ± 40 ps
τ_2	3 ± 2 ns	3.0 ± 2 ns	700 ± 40 ps	830 ± 40 ps	2.8 ± 0.2 ns	2.4 ± 0.2 ns
τ_3	30 ± 2 ns	23 ± 2 ns	4 ± 2 ns	4.0 ± 2 ns		
τ_4			15 ± 2 ns	8 ± 2 ns		

0−1, and 0−2 transitions. In contrast, **0ph** in DCM has a significantly broadened emission spectrum without a strong vibronic progression, which is characteristic of excimer formation in BPEA.[41] The emission spectrum of **1ph** is also broadened but shows a somewhat more well-defined 0−0 and 0−1 vibronic progression with maxima at 457 and 494 nm, similar to that reported for a BPEA cyclophane.[42] Dimer **2ph** has a vibronic progression similar to BPEA monomer that is red-shifted, indicating a lack of excimer formation. Although there are minor differences in the absorption spectra of the dimers between DCM and Tol, their steady state emission spectra change significantly depending on the solvent polarity (Figure S2). For example, the emission maxima of **0ph** and **1ph** are shifted more in DCM than in Tol, whereas the intensity ratio between 0 and 0 and 1−0 in Tol is greater than in DCM. Assigning the onset of the steady state absorbance and emission spectra as the first singlet excited state energy, $E(S_1)$, the BPEA monomer has the largest $E(S_1)$ = 2.60 eV followed by **2ph** (2.57 eV), **1ph** (2.55 eV), and **0ph** (2.52 eV) (Table 1). Unlike BPEA monomers, Φ_F < 1 in the BPEA dimers indicates changes to their excited state dynamics relative to the monomer.

Excited State Dynamics. We performed time-resolved fluorescence (TRF) spectroscopy to investigate the excited state dynamics of the BPEA dimers. The BPEA monomer in DCM has near-unity Φ_F with a singlet excited state lifetime of 3.2 ± 0.2 ns. On the other hand, upon photoexcitation of **0ph**, excimer formation is observed within the 40 ps instrument response function (IRF) (Figure S3). Although the identity of the species depends on the dimers, in each case, the simplest model consisted of three or four proposed states, A, B, C, and D, which are populated in a stepwise manner, was used as the kinetic model. The resulting fits represent effective rate constants that incorporate contributions from radiative decay and other pathways for population loss. By globally fitting the different time windows of the TRF spectra (Figure 2), we obtained excimer formation and decay time constants (Table 2).

Considering the spectral fits obtained from global fitting of **0ph** in DCM, we assigned species A to the excimer state due to broad spectral feature. Between species A and B, species A has an additional peak at 475 nm compared to species B (Figure 2). Presumably, species B is a structurally relaxed excimer state since there is a red-shift in the emission maximum.

Unlike in **0ph**, upon photoexcitation of **1ph** in DCM, there is a clear vibronic progression in the emission spectrum, which is assigned to the FE state (Figure 2). Following the decay of this FE state within the 40 ps IRF, we observe a broad and red-shifted emission, indicating formation of an excimer state. Besides species A, which is assigned to FE state, the rest of the states are assigned to excimer states. Once again, the multiple excimer states arise from the structural relaxation over time. The lowest energy state is reached as indicated by the most red-shifted emission (Figure S8) with its emission maximum occurring at 543 nm and having a 15 ± 2 ns lifetime. The lowest energy excimer state for **0ph** in DCM has an emission

https://dx.doi.org/10.1021/acs.jpca.0c07646
J. Phys. Chem. A 2020, 124, 8478−8487

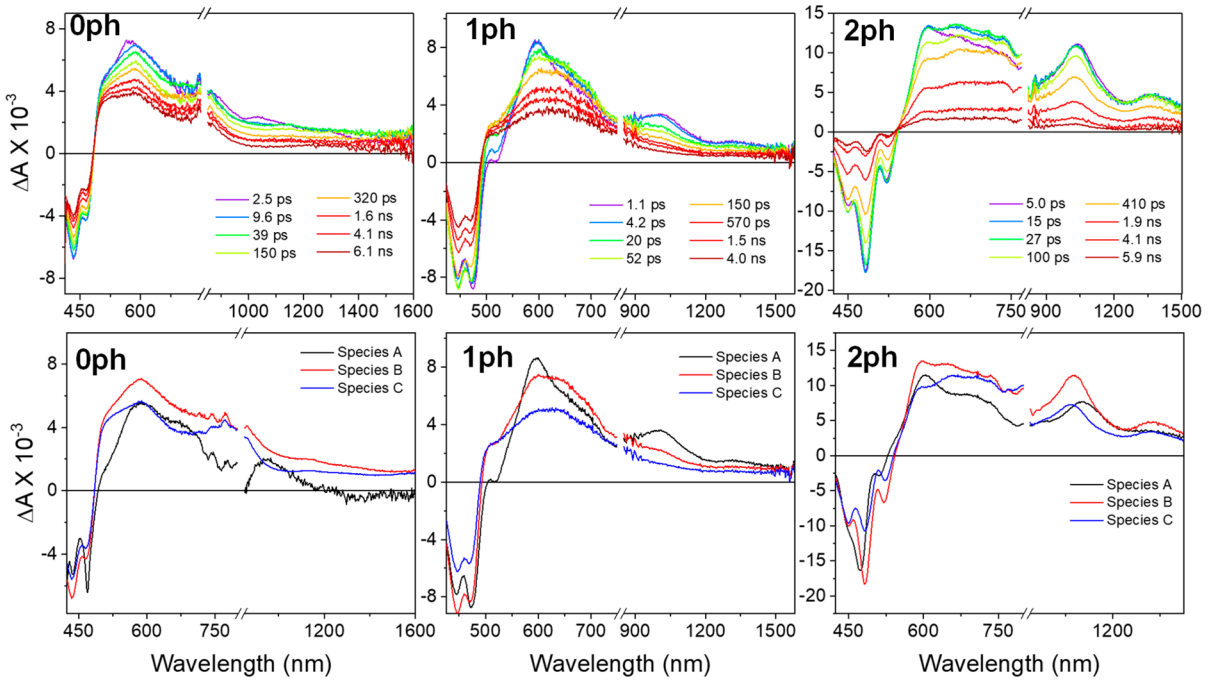

Figure 3. FsTA spectra of BPEA dimers in DCM upon photoexcitation at λ_{ex} = 414 nm (1 μJ/pulse). The fsTA spectra are globally fit by using the A → B → C → GS kinetic model, and the resulting spectral fits are shown in the bottom panel. Wavelength fits and population vs time fits are shown in Figures S13–S23.

Table 3. Excimer Formation and Decay Time Constants from TA Measurements for BPEA Dimers in DCM and Tol

	0ph DCM	**0ph** Tol	**1ph** DCM	**1ph** Tol	**2ph** DCM	**2ph** Tol
τ_1	0.4 ± 0.3 ps	0.8 ± 0.3 ps	13 ± 4 ps	42 ± 3 ps	3.0 ± 0.3 ps	2.0 ± 0.3 ps
τ_2	80 ± 5 ps	180 ± 10 ps	210 ± 40 ps	1.5 ± 0.2 ns	100 ± 10 ps	22 ± 5 ps
τ_3	31 ± 2 ns	3.4 ± 0.5 ns	3.5 ± 0.8 ns	3.6 ± 0.1 ns	3.1 ± 0.3 ns	2.3 ± 0.2 ns
τ_4		24 ± 3 ns	16 ± 4 ns	8 ± 1 ns		

maximum at 549 nm with a 30 ± 2 ns lifetime. The lower energy and longer emission lifetime of **0ph** compared to **1ph** indicate that the excimer state is more stable in **0ph**.

We also measured the TRF spectra in Tol to gauge the solvent polarity dependence of the excimer formation dynamics. There are changes in both the time constants and the emission maxima. All the excimer formation and decay time constants are slower in Tol than those in DCM for **0ph** and **1ph** (Table 2). In addition, the emission peaks are more red-shifted in DCM than in Tol, which is in good agreement with the steady state emission spectra (Figures S3–S12). Unlike **0ph** and **1ph**, **2ph** exhibits biexponential emission decays without significant spectral changes (Figure 2). If one fits the spectra using an A → B → GS model, the first decay time constant is faster in DCM than in Tol, whereas the second component remains the same.

Because the temporal resolution in our TRF experiments is limited, femtosecond transient absorption (fsTA) spectroscopy was used to investigate the excimer formation rate. Upon photoexcitation of the **0ph** dimer in DCM at 414 nm (1 μJ/pulse), a ground state bleach (GSB) and stimulated emission (SE) feature occur between 420 and 550 nm, while the singlet excited state absorption (ESA) has maxima at 588 and 955 nm (Figure 3). Following the rapid disappearance of the singlet ESA, an excimer state is formed as evident in the rise of a new ESA feature between 483 and 600 nm. If one globally fits the spectra using an A → B → C → GS model, species A shows ESA spectral features similar to the $S_n \leftarrow S_1$ transitions of the BPEA monomer. The stronger GSB of the 0–0 band at 468 nm relative to that of the 0–1 band at 436 nm further supports the assignment of species A to the singlet excited state, i.e., the FE state (Figure 3). Following rapid decay of this state, the ratio between the 0–0 and 0–1 bands also changes to that typical of an H-type aggregate in species B. Both species B and C are the ESA of the excimer state. The spectral features of species B and C are similar, but a major difference exists in the ratio of the peak at 588 nm to the shoulder at 503 nm. From the global fitting, the excimer formation time constant is 0.4 ± 0.3 ps, with two different excimer decay time constants of 80 ± 5 ps and 31 ± 2 ns (Table 3). These values are in good agreement with those obtained from the TRF measurements. The same analysis was performed on **0ph** in Tol, and the resulting spectral fits are shown in Figure S15. Both the excimer formation and the decay time constants are slower than those of **0ph** in DCM as reported in Table 3.

Similarly, in **1ph**, the early time features result from the singlet excited or FE state. There is a pronounced GSB and SE at 400–500 nm, where the 0–0 peak is more intense than 0–1 peak along with ESA maxima at 597 and 1024 nm. If one globally fits the spectra using an A → B → C → D → GS model, the excimer formation time constant is τ = 13 ± 4 ps, followed by the three different excimer decay time constants (Table 3). These decay time constants are in good agreement with those obtained from TRF measurements. The overall slow formation and decay time constants of the excimer in Tol indicate that the excited state dynamics of these dimers are

https://dx.doi.org/10.1021/acs.jpca.0c07646
J. Phys. Chem. A 2020, 124, 8478–8487

solvent polarity dependent. In addition, compared to **0ph**, the excimer formation rate is significantly slower in **1ph**, and thus, a clear singlet or FE state ESA is observed in species A.

In the case of **2ph**, the overall ESA spectra have a more pronounced vibronic progressions. If one globally fits the spectra using an A → B → GS model, species A results from the singlet excited state and has an ESA with local maxima at 603, 1076, and 1391 nm. Species B has a new spectral feature at 650 nm, which is assigned to the BPEA anion based on its spectral similarity to the chemically reduced BPEA monomer.[43] In addition, this anion spectral feature is more pronounced in **2ph** in DMF, which is a higher polarity solvent than DCM (Figure S23). We attribute this anion feature to a small degree of symmetry-breaking charge separation (SB-CS). Species C has spectral features similar to species B but with a decreased amplitude. For **2ph** in Tol, the overall spectral features do not change over time, indicating that SB-CS is absent and the multiple decay time constants are attributed to solvation and multiple conformers. Regardless, SB-CS is a minor decay pathway given the high Φ_F of **2ph** in all three solvents. The Φ_F of **2ph** in Tol is 90 ± 5% and 82 ± 9% in DCM and 77 ± 3% in DMF. Such decreasing Φ_F and more pronounced anion feature with increasing solvent polarity strongly support the presence of minor SB-CS in **2ph**. In addition to the decrease in Φ_F, there is also a red-shift in the emission spectrum in DMF and a stronger 0−1 vibronic peak compared to Tol and DCM (Figure S2).

Quantifying FE and CT Contributions to the Excimer State. Based on the results from fsTA and TRF spectroscopies, there is a significant solvent dependence in the excited state dynamics of the BPEA dimers. Faster excimer formation and slower decay dynamics are observed in higher dielectric environments for **0ph** and **1ph**. In addition, SB-CS is only observable in high-polarity solvents for **2ph**. To further understand these changes in excited state dynamics, we calculated the contribution of FE and CT character in the excimer state by diagonalizing the following electronic Hamiltonian matrix:

$$H_{el} = \begin{bmatrix} E_{S1} & J_{Coul} & V_{HH} & V_{LL} \\ J_{Coul} & E_{S1} & V_{LL} & V_{HH} \\ V_{HH} & V_{LL} & E_{CT} & 0 \\ V_{LL} & V_{HH} & 0 & E_{CT} \end{bmatrix} \quad (2)$$

where J_{Coul} is the strength of Coulombic interaction and V_{HH} and V_{LL} are the hole and electron transfer integrals for the two BPEA molecules in the dimer. Here, the four basis states are S_0S_1, S_1S_0, CA, and AC, and diagonalizing this Hamiltonian matrix results in four excimer eigenstates. The detailed description is given in the Supporting Information. Diagonalizing this electronic Hamiltonian provides four excimer eigenstates with the corresponding energies shown in the Supporting Information. Because the lowest energy state presumably has the highest population, we compare the FE and CT contribution which are shown as $|a|^2/(a|^2 + b|^2)$ and $|b|^2/(a|^2 + b|^2)$, respectively, in Table 4.

Comparing the CT contributions, among the BPEA dimers in DCM, **0ph** has the greatest CT contribution (0.16) followed by **1ph** (0.08) and **2ph** (0.06). Although this trend is similar across the dimers in Tol, the magnitude of the ratio is significantly greater than those in DCM. Such a result is reasonable because in a low-polarity solvent like Tol, the CT state energy is higher; thus, there is poorer mixing of the CT state with the FE state in Tol. In addition, the energy of the excimer state (Table 4) decreases with an increasing CT contribution. Thus, **0ph** has both the greatest CT contribution and the lowest excimer state energy.

Table 4. Calculated Values of FE and CT Contributions and the Excimer State Energies in DCM and Tol

	0ph DCM	0ph Tol	1ph DCM	1ph Tol	2ph DCM	2ph Tol
$\|a\|^2/(a\|^2 + b\|^2)$	0.84	0.997	0.92	0.998	0.94	0.998
$\|b\|^2/(a\|^2 + b\|^2)$	0.16	0.003	0.08	0.002	0.06	0.002
$\|a\|^2/\|b\|^2$	5.1	125	12	416	15	543
energy (eV)	2.27	2.29	2.30	2.31	2.30	2.31

DISCUSSION

Comparison between Experimental Rates and the Calculated Exciton Coupling. There is good qualitative agreement for all BPEA dimers between the experimentally observed excimer formation rates and the CT contributions. Based on the fsTA and TRF spectroscopy results, **0ph** has the fastest excimer formation rate (Table 1) and also has the greatest CT contribution. The greater CT contribution in **1ph** allows facile excimer formation, whereas **2ph** behaves like the BPEA monomer with a small degree of CT. However, it is unclear how the CT contribution affects SB-CS.

Based on the calculated coefficients, the greater degree of CT contribution, i.e., larger $|b|^2/(a|^2 + |b|^2)$ values, leads to lowering of the CT state energies. Experimentally, lower energy excimer state emission is observed from **0ph** (2.25 eV) compared to **1ph** (2.29 eV). From the calculations, **0ph** has the lower excimer state energy (2.27 eV) compared to **1ph** (2.30 eV) in DCM. Thus, the calculations show that increasing the CT contribution lowers the excimer state energy, and moreover, there is a near quantitative agreement between the experimentally observed excimer state energy and the calculated energy. A similar trend is also seen in Tol. It should be noted that the excimer state energy is similar across different dimers, but their dynamics are significantly different due to changes in electronic coupling.

Comparing the Results for BPEA Dimers to Those for Other Chromophores. Because the CT contribution provides rich information about BPEA dimer systems, we have also calculated these values for different systems that form excimers such as the crystalline DPP system and PDI covalent dimers in solution (Figure 4). Previous studies have shown that a selection of DPP systems undergo SF via an excimer intermediate state.[18,44,45] Different crystal packing structures lead to changes in electronic coupling and result in excimer-mediated SF or direct SF from the singlet excited state. Among different DPP derivatives, the *n*-hexyl (**C6**) derivative forms excimers with the fastest rate followed by methyl (**Me**) and triethylene glycol (**TEG**) derivatives.[18] In contrast, the phenyl-DPP (**Ph**) derivative undergoes SF without an excimer intermediate state.[44] Comparing the CT contributions for DPP systems, **C6** has the greatest value of 0.13 followed by **Me** (0.04), **TEG** (0.009), and **Ph** (0.0005) (see Tables S14−S17). This trend is also seen in the excimer formation rate where the fastest rate occurs in **C6** $(\sim 0.9\ ps)^{-1}$ followed by **Me** $(\sim 2.7\ ps)^{-1}$ and **TEG** $(\sim 10.1\ ps)^{-1}$.[18] Similar to BPEA dimers, a greater CT contribution lowers the excimer state energy as

https://dx.doi.org/10.1021/acs.jpca.0c07646
J. Phys. Chem. A 2020, 124, 8478−8487

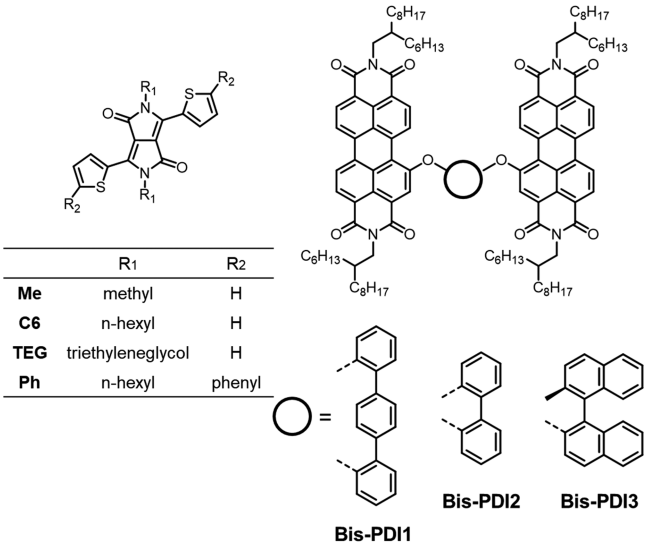

Figure 4. Previously reported polycrystalline DPP and PDI covalent dimers. These systems are used to calculate FE and CT contributions in this work.

evidenced by **C6** having the lowest excimer state energy of 2.00 eV followed by **Me** (2.15 eV), **TEG** (2.16 eV), and **Ph** (2.42 eV). All these trends in the DPP system further support the idea that excimer formation is facilitated by a greater CT contribution, and when there is a lack of CT contribution as shown in the **Ph** derivative, excimer formation is inhibited.

In the case of PDI covalent dimers (Figure 4), **Bis-PDI1** has a CT contribution of 0.14, whereas **Bis-PDI2** and **Bis-PDI3** have the ratios of 0.59 and 0.58, respectively (Tables S18–S20). **Bis-PDI1** forms excimers in <200 fs, whereas **PDI2** and **PDI3** form a mixed state in ~50 ps, which is composed of $^1(S_0S_1)$, $^1(T_1T_1)$, and CT states, similar to the mixed state observed in terrylenediimide (TDI) dimers.[46] The **PDI2** and **PDI3** dimers are unique cases because the lowest excimer eigenstate has a greater contribution from the CT state than the FE state. Kim and co-workers suggest that a comparable contribution of FE and CT states prevents excimer formation but rather facilitates multiexciton generation.[5] On the other hand, the **PDI1** dimer, which forms excimers rapidly, still has a greater contribution from FE similar to the BPEA covalent dimers and some of the DPP systems.

Based on the FE and CT contributions calculated in variety of dimer systems including BPEA, PDI, and DPP, there seems to be a threshold for a CT contribution to facilitate excimer formation (Figure 5). For instance, in the BPEA covalent dimers, when the CT contribution is less than 0.06, the excimer state does not form as seen in **2ph**, setting the lower limit of CT contribution for excimer formation. In crystalline DPP systems, the threshold for CT contribution is much smaller, below 0.0005 for prohibiting excimer formation. In contrast, for the covalent PDI dimers, **PDI2** and **PDI3**, when the CT contribution is significant (0.58), exceeding the contribution of FE, there is also no formation of excimer state, setting the upper limit of CT contribution for excimer formation. Although the exact value of these thresholds varies among different systems, there appears to be a specific range of CT contributions to facilitate excimer formation within the same series of molecules.

Absence of Singlet Fission. Based on the singlet ($E(S_1)$ = 2.52–2.60 eV) and triplet excited state energies ($E(T_1)$ = 1.24–1.30 eV), the latter of which were obtained by using multiple triplet sensitizers[47] (see the Supporting Information), BPEA covalent dimers have favorable energetics for SF; however, unlike BPEA in the solid state, where efficient SF occurs, either excimer formation or fluorescence is a major decay pathway in the covalent BPEA dimers. There are two reasons. First, the excimer formation rate is much faster than the SF rate observed in the solid state film due to a larger degree of CT contribution in BPEA dimers compared to solid state BPEA. We calculated the CT contributions for both the *C*2/*c* (0.02) and *Pbcn* (0.005) polymorphs of BPEA in solid state films (Figure 5). These values are far smaller than the CT contribution observed in **2ph**, which is 0.06, and thus it is reasonable that there is no excimer formation in *C*2/*c* and *Pbcn* BPEA films.

Second, presumably for SF to occur in covalent dimers, there needs to be a significant contribution from the CT state as seen in the **PDI2** and **PDI3** dimers. Both **PDI2** and **PDI3** have CT contributions that are larger than those of FE, and only these two dimers undergo SF. In addition, upon photoexcitation of TDI dimers, a spectroscopically observable mixed state composed of $^1(S_0S_1)$, $^1(T_1T_1)$, and CT states is formed.[46] Because of a large CT state contribution, both cation and anion species are spectroscopically observable in TDI dimers.[46] Similarly, in pentacene systems, where ultrafast SF occurs, the CT character is calculated to range from 50% to

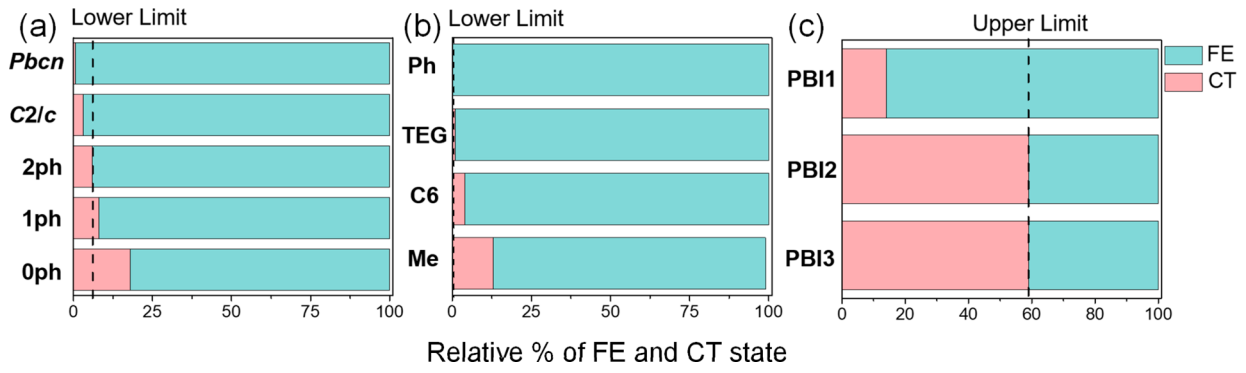

Figure 5. Calculated percent contribution of FE and CT states. The lower limit of the CT contribution for excimer formation is shown as a dashed line for the (a) BPEA and (b) DPP systems, and the upper limit is shown for the (c) PDI systems. The calculated FE and CT contributions are shown in Table S21.

https://dx.doi.org/10.1021/acs.jpca.0c07646
J. Phys. Chem. A 2020, 124, 8478–8487

94%.[48] Thus, in BPEA covalent dimers, the CT contribution is insufficient to drive SF, but it also exceeds the threshold necessary for the CT contribution to promote excimer formation. Presumably, the CT contribution can be balanced in specific molecular designs to avoid excimer formation and to promote SF.

CONCLUSIONS

We have synthesized covalent BPEA dimers using a xanthene bridge and changed the longitudinal distance between the two BPEA units by changing the number of phenyl spacers. Based on fsTA and TRF measurements, excimer formation is a major decay pathway for **0ph** and **1ph**, whereas fluorescence emission from the S_1 state with a small degree of SB-CS is observed for **2ph**. Solvent-polarity-dependent excited state dynamics confirms the importance of the CT state in excimer formation. We quantified the contribution of the FE and CT states and found that there are different lower and upper thresholds in the CT contribution among different systems including BPEA, DPP, and PDI molecular aggregates that facilitate excimer state formation. Such quantitative analysis using exciton coupling could aid in designing molecular aggregates to avoid excimer state formation and to favor singlet fission.

ASSOCIATED CONTENT

Supporting Information

The Supporting Information is available free of charge at https://pubs.acs.org/doi/10.1021/acs.jpca.0c07646.

Synthesis and characterization of **1ph** and **2ph**, additional fsTA and nsTA spectroscopy and kinetic analysis, time-resolved fluorescence spectroscopy, triplet spectra, and computational data (PDF)

AUTHOR INFORMATION

Corresponding Author

Michael R. Wasielewski − *Department of Chemistry and Institute for Sustainability and Energy at Northwestern, Northwestern University, Evanston, Illinois 60208-3113, United States;* orcid.org/0000-0003-2920-5440; Email: m-wasielewski@northwestern.edu

Authors

Youn Jue Bae − *Department of Chemistry and Institute for Sustainability and Energy at Northwestern, Northwestern University, Evanston, Illinois 60208-3113, United States;* orcid.org/0000-0003-4006-2292

Daiki Shimizu − *Department of Chemistry and Institute for Sustainability and Energy at Northwestern, Northwestern University, Evanston, Illinois 60208-3113, United States; Department of Chemistry, Graduate School of Science, Kyoto University, Kyoto 606-8502, Japan;* orcid.org/0000-0002-2053-3483

Jonathan D. Schultz − *Department of Chemistry and Institute for Sustainability and Energy at Northwestern, Northwestern University, Evanston, Illinois 60208-3113, United States;* orcid.org/0000-0002-3386-5460

Gyeongwon Kang − *Department of Chemistry and Institute for Sustainability and Energy at Northwestern, Northwestern University, Evanston, Illinois 60208-3113, United States;* orcid.org/0000-0002-8219-2717

Jiawang Zhou − *Department of Chemistry and Institute for Sustainability and Energy at Northwestern, Northwestern University, Evanston, Illinois 60208-3113, United States;* orcid.org/0000-0002-2399-0030

George C. Schatz − *Department of Chemistry and Institute for Sustainability and Energy at Northwestern, Northwestern University, Evanston, Illinois 60208-3113, United States;* orcid.org/0000-0001-5837-4740

Atsuhiro Osuka − *Department of Chemistry, Graduate School of Science, Kyoto University, Kyoto 606-8502, Japan;* orcid.org/0000-0001-8697-8488

Complete contact information is available at: https://pubs.acs.org/10.1021/acs.jpca.0c07646

Notes

The authors declare no competing financial interest.

ACKNOWLEDGMENTS

This work was supported by the U.S. Department of Energy, Office of Science, Office of Basic Energy Sciences, under Award DE-FG02-99ER14999 (M.R.W.). G.K. and G.C.S. were supported by U.S. Department of Energy, Office of Science, Office of Basic Energy Sciences, under Award DE-SC000475. Y.B. gratefully acknowledges support from the Ryan Fellowship and the International Institute for Nanotechnology at Northwestern University. D.S. acknowledges a JSPS fellowship for young scientists and Grant-in-Aid for Scientific Research on Innovative Areas MEXT, "Science of Atomic Layers (SATL)". J.D.S. acknowledges support from the National Science Foundation Graduate Research Fellowship Program under Grant DGE-1842165. This work made use of the IMSERC at Northwestern University, which has received support from the Soft and Hybrid Nanotechnology Experimental (SHyNE) Resource (NSF ECCS-1542205), the State of Illinois, and the International Institute for Nanotechnology (IIN).

REFERENCES

(1) Young, R. M.; Wasielewski, M. R. Mixed electronic states in molecular dimers: Connecting singlet fission, excimer formation and symmetry-breaking charge transfer. *Acc. Chem. Res.* **2020**, *53*, 1957−1968.

(2) Margulies, E. A.; Shoer, L. E.; Eaton, S. W.; Wasielewski, M. R. Excimer formation in cofacial and slip-stacked perylene-3,4:9,10-bis(dicarboximide) dimers on a redox-inactive triptycene scaffold. *Phys. Chem. Chem. Phys.* **2014**, *16*, 23735−23742.

(3) Cook, R. E.; Phelan, B. T.; Kamire, R. J.; Majewski, M. B.; Young, R. M.; Wasielewski, M. R. Excimer formation and symmetry-breaking charge transfer in cofacial perylene dimers. *J. Phys. Chem. A* **2017**, *121*, 1607−1615.

(4) Sung, J.; Kim, P.; Fimmel, B.; Würthner, F.; Kim, D. Direct observation of ultrafast coherent exciton dynamics in helical π-stacks of self-assembled perylene bisimides. *Nat. Commun.* **2015**, *6*, 8646.

(5) Hong, Y.; Kim, J.; Kim, W.; Kaufmann, C.; Kim, H.; Würthner, F.; Kim, D. Efficient multiexciton state generation in charge-transfer-coupled perylene bisimide dimers via structural control. *J. Am. Chem. Soc.* **2020**, *142*, 7845−7857.

(6) Myong, M. S.; Zhou, J.; Young, R. M.; Wasielewski, M. R. Charge-transfer character in excimers of perylenediimides self-assembled on anodic aluminum oxide membrane walls. *J. Phys. Chem. C* **2020**, *124*, 4369−4377.

(7) Walker, B. J.; Musser, A. J.; Beljonne, D.; Friend, R. H. Singlet exciton fission in solution. *Nat. Chem.* **2013**, *5*, 1019−1024.

(8) Pensack, R. D.; Ashmore, R. J.; Paoletta, A. L.; Scholes, G. D. The nature of excimer formation in crystalline pyrene nanoparticles. *J. Phys. Chem. C* **2018**, *122*, 21004−21017.

(9) Margulies, E. A.; Logsdon, J. L.; Miller, C. E.; Ma, L.; Simonoff, E.; Young, R. M.; Schatz, G. C.; Wasielewski, M. R. Direct observation of a charge-transfer state preceding high-yield singlet fission in terrylenediimide thin films. *J. Am. Chem. Soc.* **2017**, *139*, 663−671.
(10) Vollbrecht, J. Excimers in organic electronics. *New J. Chem.* **2018**, *42*, 11249−11254.
(11) Chen, Z.; Stepanenko, V.; Dehm, V.; Prins, P.; Siebbeles, L. D. A.; Seibt, J.; Marquetand, P.; Engel, V.; Würthner, F. Photoluminescence and conductivity of self-assembled $\pi-\pi$ stacks of perylene bisimide dyes. *Chem. - Eur. J.* **2007**, *13*, 436−449.
(12) Singh, R.; Kim, M.; Lee, J.-J.; Ye, T.; Keivanidis, P. E.; Cho, K. Excimer formation effects and trap-assisted charge recombination loss channels in organic solar cells of perylene diimide dimer acceptors. *J. Mater. Chem. C* **2020**, *8*, 1686−1696.
(13) Wasielewski, M. R. Self-assembly strategies for integrating light harvesting and charge separation in artificial photosynthetic systems. *Acc. Chem. Res.* **2009**, *42*, 1910−1921.
(14) Matsui, A. H. Excitonic processes in aromatic molecular crystals of strong exciton-phonon coupling. *Pure Appl. Chem.* **1995**, *67*, 429−436.
(15) Fink, R. F.; Seibt, J.; Engel, V.; Renz, M.; Kaupp, M.; Lochbrunner, S.; Zhao, H.-M.; Pfister, J.; Würthner, F.; Engels, B. Exciton trapping in π-conjugated materials: A quantum-chemistry-based protocol applied to perylene bisimide dye aggregates. *J. Am. Chem. Soc.* **2008**, *130*, 12858−12859.
(16) Dover, C. B.; Gallaher, J. K.; Frazer, L.; Tapping, P. C.; Petty, A. J., II; Crossley, M. J.; Anthony, J. E.; Kee, T. W.; Schmidt, T. W. Endothermic singlet fission is hindered by excimer formation. *Nat. Chem.* **2018**, *10*, 305−310.
(17) Brown, K. E.; Salamant, W. A.; Shoer, L. E.; Young, R. M.; Wasielewski, M. R. Direct observation of ultrafast excimer formation in covalent perylenediimide dimers using near-infrared transient absorption spectroscopy. *J. Phys. Chem. Lett.* **2014**, *5*, 2588−2593.
(18) Mauck, C. M.; Hartnett, P. E.; Margulies, E. A.; Ma, L.; Miller, C. E.; Schatz, G. C.; Marks, T. J.; Wasielewski, M. R. Singlet fission via an excimer-like intermediate in 3,6-bis(thiophen-2-yl)-diketopyrrolopyrrole derivatives. *J. Am. Chem. Soc.* **2016**, *138*, 11749−11761.
(19) Sung, J.; Nowak-Król, A.; Schlosser, F.; Fimmel, B.; Kim, W.; Kim, D.; Würthner, F. Direct observation of excimer-mediated intramolecular electron transfer in a cofacially-stacked perylene bisimide pair. *J. Am. Chem. Soc.* **2016**, *138*, 9029−9032.
(20) Azumi, T.; Armstrong, A. T.; McGlynn, S. P. Energy of excimer luminescence. II. Configuration interaction between molecular exciton states and charge resonance states. *J. Chem. Phys.* **1964**, *41*, 3839−3852.
(21) Kim, W.; Nowak-Król, A.; Hong, Y.; Schlosser, F.; Würthner, F.; Kim, D. Solvent-modulated charge-transfer resonance enhancement in the excimer state of a bay-substituted perylene bisimide cyclophane. *J. Phys. Chem. Lett.* **2019**, *10*, 1919−1927.
(22) Wu, Y.; Zhou, J.; Phelan, B. T.; Mauck, C. M.; Stoddart, J. F.; Young, R. M.; Wasielewski, M. R. Probing distance dependent charge-transfer character in excimers of extended viologen cyclophanes using femtosecond vibrational spectroscopy. *J. Am. Chem. Soc.* **2017**, *139*, 14265−14276.
(23) Kasha, M.; Rawls, H. R.; El-Bayoumi, M. A. The exciton model in molecular spectroscopy. *Pure Appl. Chem.* **1965**, *11*, 371−392.
(24) Hestand, N. J.; Spano, F. C. Molecular aggregate photophysics beyond the kasha model: Novel design principles for organic materials. *Acc. Chem. Res.* **2017**, *50*, 341−350.
(25) Kaufmann, C.; Bialas, D.; Stolte, M.; Würthner, F. Discrete π-stacks of perylene bisimide dyes within folda-dimers: Insight into long- and short-range exciton coupling. *J. Am. Chem. Soc.* **2018**, *140*, 9986−9995.
(26) Bae, Y. J.; Christensen, J. A.; Kang, G.; Zhou, J.; Young, R. M.; Wu, Y.-L.; Van Duyne, R. P.; Schatz, G. C.; Wasielewski, M. R. Substituent effects on energetics and crystal morphology modulate singlet fission in 9,10-bis(phenylethynyl)anthracenes. *J. Chem. Phys.* **2019**, *151*, 044501.
(27) Bae, Y. J.; Christensen, J. A.; Kang, G.; Malliakas, C. D.; Zhou, J.; Nelson, J. N.; Young, R. M.; Wu, Y. L.; van Duyne, R. P.; Schatz, G. C.; Wasielewski, M. R. Design principles for efficient singlet fission in anthracene-based organic semiconductors. *Proc. SPIE 11084, Physical Chemistry of Semiconductor Materials and Interfaces XVIII* **2019**, *110840Q*.
(28) Bae, Y. J.; Kang, G.; Malliakas, C. D.; Nelson, J. N.; Zhou, J.; Young, R. M.; Wu, Y. L.; Van Duyne, R. P.; Schatz, G. C.; Wasielewski, M. R. Singlet fission in 9,10-bis(phenylethynyl)-anthracene thin films. *J. Am. Chem. Soc.* **2018**, *140*, 15140−15144.
(29) Young, R. M.; Dyar, S. M.; Barnes, J. C.; Juricek, M.; Stoddart, J. F.; Co, D. T.; Wasielewski, M. R. Ultrafast conformational dynamics of electron transfer in exbox$^{4+}\subset$perylene. *J. Phys. Chem. A* **2013**, *117*, 12438−12448.
(30) Greenfield, S. R.; Wasielewski, M. R. Near-transform-limited visible and near-ir femtosecond pulses from optical parametric amplification using type II β-barium borate. *Opt. Lett.* **1995**, *20*, 1394−1396.
(31) Tempelaar, R.; Reichman, D. R. Vibronic exciton theory of singlet fission. I. Linear absorption and the anatomy of the correlated triplet pair state. *J. Chem. Phys.* **2017**, *146*, 174703.
(32) Hestand, N. J.; Spano, F. C. Interference between coulombic and ct-mediated couplings in molecular aggregates: H- to J-aggregate transformation in perylene-based π-stacks. *J. Chem. Phys.* **2015**, *143*, 244707.
(33) Friedrich, D. M.; Mathies, R.; Albrecht, A. C. Studies of excited electronic states of anthracene and some of its derivatives by photoselection and PPP-SCF calculations. *J. Mol. Spectrosc.* **1974**, *51*, 166−188.
(34) Benkyi, I.; Tapavicza, E.; Fliegl, H.; Sundholm, D. Calculation of vibrationally resolved absorption spectra of acenes and pyrene. *Phys. Chem. Chem. Phys.* **2019**, *21*, 21094−21103.
(35) te Velde, G.; Bickelhaupt, F. M.; Baerends, E. J.; Fonseca Guerra, C.; van Gisbergen, S. J. A.; Snijders, J. G.; Ziegler, T. Chemistry with ADF. *J. Comput. Chem.* **2001**, *22*, 931−967.
(36) Senthilkumar, K.; Grozema, F. C.; Bickelhaupt, F. M.; Siebbeles, L. D. A. Charge transport in columnar stacked triphenylenes: Effects of conformational fluctuations on charge transfer integrals and site energies. *J. Chem. Phys.* **2003**, *119*, 9809−9817.
(37) Renaud, N.; Sherratt, P. A.; Ratner, M. A. Mapping the relation between stacking geometries and singlet fission yield in a class of organic crystals. *J. Phys. Chem. Lett.* **2013**, *4*, 1065−1069.
(38) Mauck, C. M.; Bae, Y. J.; Chen, M.; Powers-Riggs, N.; Wu, Y.-L.; Wasielewski, M. R. Charge-transfer character in a covalent diketopyrrolopyrrole dimer: Implications for singlet fission. *ChemPhotoChem.* **2018**, *2*, 223−233.
(39) McCarthy, B. D.; Hontz, E. R.; Yost, S. R.; Van Voorhis, T.; Dincă, M. Charge transfer or J-coupling? Assignment of an unexpected red-shifted absorption band in a naphthalenediimide-based metal−organic framework. *J. Phys. Chem. Lett.* **2013**, *4*, 453−458.
(40) Levitus, M.; Garcia-Garibay, M. A. Polarized electronic spectroscopy and photophysical properties of 9,10-bis-(phenylethynyl)anthracene. *J. Phys. Chem. A* **2000**, *104*, 8632−8637.
(41) Yamane, S.; Sagara, Y.; Kato, T. Steric effects on excimer formation for photoluminescent smectic liquid-crystalline materials. *Chem. Commun.* **2013**, *49*, 3839−3841.
(42) Sagara, Y.; Simon, Y. C.; Tamaoki, N.; Weder, C. A mechano- and thermoresponsive luminescent cyclophane. *Chem. Commun.* **2016**, *52*, 5694−5697.
(43) Winters, M. U.; Pettersson, K.; Mårtensson, J.; Albinsson, B. Competition between superexchange-mediated and sequential electron transfer in a bridged donor−acceptor system. *Chem. - Eur. J.* **2005**, *11*, 562−573.
(44) Hartnett, P. E.; Margulies, E. A.; Mauck, C. M.; Miller, S. A.; Wu, Y.; Wu, Y.-L.; Marks, T. J.; Wasielewski, M. R. Effects of crystal morphology on singlet exciton fission in diketopyrrolopyrrole thin films. *J. Phys. Chem. B* **2016**, *120*, 1357−1366.

https://dx.doi.org/10.1021/acs.jpca.0c07646
J. Phys. Chem. A 2020, 124, 8478−8487

(45) Miller, C. E.; Wasielewski, M. R.; Schatz, G. C. Modeling singlet fission in rylene and diketopyrrolopyrrole derivatives: The role of the charge transfer state in superexchange and excimer formation. *J. Phys. Chem. C* **2017**, *121*, 10345−10350.
(46) Chen, M.; Bae, Y. J.; Mauck, C. M.; Mandal, A.; Young, R. M.; Wasielewski, M. R. Singlet fission in covalent terrylenediimide dimers: Probing the nature of the multiexciton state using femtosecond mid-infrared spectroscopy. *J. Am. Chem. Soc.* **2018**, *140*, 9184−9192.
(47) Galstyan, A.; Maurya, Y. K.; Zhylitskaya, H.; Bae, Y. J.; Wu, Y.-L.; Wasielewski, M. R.; Lis, T.; Dobrindt, U.; Stępień, M. π-Extended donor−acceptor porphyrins and metalloporphyrins for antimicrobial photodynamic inactivation. *Chem. - Eur. J.* **2020**, *26*, 8262−8266.
(48) Monahan, N.; Zhu, X. Y. Charge transfer−mediated singlet fission. *Annu. Rev. Phys. Chem.* **2015**, *66*, 601−618.

https://dx.doi.org/10.1021/acs.jpca.0c07646
J. Phys. Chem. A 2020, 124, 8478−8487